

ARTICLE TYPE

Constrained output feedback control of spacecraft attitude via explicit reference governor

Qingqing Dang¹ | Zhenbao Liu¹ | Ali Zemouche² | Ping Liu³ | Fan Zhang^{*3}

¹ School of Civil Aviation, Northwestern Polytechnical University, Xi'an, China

² Université de Lorraine, CRAN UMR CNRS 7039, Cosnes-et-Romain, France

³ School of Aeronautics and Astronautics, Sun Yat-sen University, Shenzhen, China

Correspondence

*Corresponding F. Zhang, Email: zhangfan6@mail.sysu.edu.cn

Summary

This paper proposes an explicit reference governor-based control scheme for the velocity-free spacecraft attitude maneuver problem subject to the pointing constraint, the angular velocity constraint, and the input constraint. The proposed two-layer control scheme guarantees asymptotic stability of the attitude while satisfying the aforementioned constraints. The inner layer relies on output feedback control via an immersion and invariance technology-based angular velocity observer, enabling attitude stabilization without measuring angular velocity. By analyzing the geometry of the pointing constraint, the upper bound of the angular velocity, and the optimization solution of the control input, the safety boundary described by the invariant set is obtained in the reference layer. Additionally, we introduce the dynamic factor related to the angular velocity estimation error into the invariant set to prevent states from exceeding the constraint set due to unmeasurable angular velocity information. The shortest guidance path is then designed in the reference layer. Finally, we verify the effectiveness of the proposed constrained attitude control algorithm through numerical simulations.

KEYWORDS:

attitude maneuver, constraints, explicit reference governor, angular velocity observer

1 | INTRODUCTION

Spacecraft attitude maneuver plays a significant role in complex space autonomous missions^{1,2,3}. Restricted by the actuators and sensitive payloads, the attitude maneuver algorithms are often required to achieve system stability while simultaneously satisfying various constraints. For example, the spacecraft is usually required to maneuver from one state to another with the time limitation, while keeping its star sensor avoid from the bright objects (e.g. earth) and preventing the command torque from exceeding the capacity of the actuator⁴. These missions can be regarded as spacecraft maneuver under state and control constraints^{4,5,6}. Furthermore, due to the failure of gyroscopes, the angular velocity information may be unavailable. Therefore, constrained velocity-free attitude control is an issue of great theoretical and practical importance.

For attitude control systems with actuator saturation, if the input constraints are not considered in the controller design explicitly, although the performance is affected by the input limitation, its stability sometimes can still be proved theoretically⁷. The traditional controller designed directly using the Lyapunov function cannot restrict the state trajectories. Hence, the attitude commands are used in the attitude maneuver path design in the presence of multiple attitude constraints^{4,8}. This strategy can effectively solve part of the engineering problems, but the flexibility is poor and it is difficult to meet the tasks with high real-time dynamic requirements. To deal with the actuator saturation, control bandwidth limit, slew rate limit, and/or eigenaxis

slew constraints, the saturation function and integrate function are introduced in a nonlinear feedback control logic by Wie et al. for the rapid re-targeting control of agile spacecraft⁹. This method can handle single-axis maneuvers with particular constraints well, but it is difficult to handle three-axis maneuvers with complex constraints.

Potential functions together with Lyapunov functions can handle complex constraints, which provide a promising technology for the constrained attitude control problem^{10,11,12,13}. Lee et al.¹⁰ constructed a strictly convex logarithmic barrier potential for attitude-constrained zones by utilizing a convex parameterization technology. Inspired by 10 and using the anti-unwinding attitude error function, a new algorithm for the attitude reorientation guidance under forbidden pointing constraints is proposed in 14. In addition, Shen et al.¹⁵ dealt with rest-to-rest three-axis attitude reorientation under multiple attitude-constraint zones and angular velocity limits via a quadratic potential function and a logarithmic potential function. However, it is difficult to simultaneously handle different types of complex constraints by the potential functions based constrained control algorithm. Since the potential function is constructed in the Lyapunov function and the convergence of Lyapunov function is the result of the convergence game between potential function and states, the robustness of the system may become worse.

Trajectory optimization methods, such as model predictive control (MPC), can also address constrained control issues. In 16 and 17, MPC on SO(3) has been developed for constrained attitude maneuver of a fully actuated spacecraft. However, it needs to optimize the function at each sampling horizon in MPC, which limits its application in fast response systems, for example spacecraft maneuver.

Recently, a novel add-on control scheme called explicit reference governor (ERG) was introduced by Nicotra et al.^{18,19,20}. The key idea is to augment a pre-stabilized system with a control unit and manipulates the auxiliary reference to ensure constraint satisfaction, which means the stability and the constraint issues can be handled separately. Then, This control technology has been applied to the Unmanned Aerial Vehicles and spacecraft attitude control problems with state constraints^{21,22,6}. Another challenge in attitude control is the velocity-free control problem besides the constraints. This issue has attracted many researchers and has been well studied²³, for example the immersion and invariance (I&I) based globally exponentially convergent observer is utilized to conduct the angular velocity observer^{7,24,25}. However, the velocity-free attitude maneuver problem in the presence of constraints was studied in just a few works. For example, a velocity-free attitude reorientation control law with pointing constraints is established in 26.

Inspired by the ERG and the I&I technologies²⁷, a constrained velocity-free control algorithm for spacecraft reorientation is presented in this paper, where the attitude pointing, angular velocity, and control input constraints are considered. The attitude dynamics as well as various constraints are formulated in terms of modified Rodrigues parameters (MRPs). The MRPs constitute a singular, nonunique and minimal parametrization set of the three-dimensional special orthogonal group SO(3). Fortunately, the singularity can be avoided by using the nonuniqueness properties through switching the parameters between MRPs and its shadow at the unit sphere^{28,29}. Then, the ERG-based control scheme is deduced where the output controller based on the angular velocity observer is designed in the inner loop firstly. To the best of the authors' knowledge, the result presented in this paper is the first attempt to address the observer-based attitude maneuver issue with pointing constraints, angular velocity constraints, and input constraints. Finally, the performance and robustness of the proposed algorithm is verified by the numerical simulations and Monte Carlo simulations.

2 | PRELIMINARIES

2.1 | Spacecraft attitude kinematics and dynamics

The MRPs vector is defined in terms of an Euler rotation angle $\phi \in \mathbb{R}$ about the principal axis $\{\mathbf{n} | \mathbf{n}^T \mathbf{n} = 1, \mathbf{n} \in \mathbb{R}^3\}$. Let \mathcal{F}_B be the body-fixed frame, and \mathcal{F}_I be the inertial frame. Then, the attitude with respect to the inertial frame can be described by MRPs and given by $\sigma_{BI} = \mathbf{n}_{BI} \tan(\phi_{BI}/4)$. The attitude kinematics and dynamics of the rigid-body spacecraft are given by³⁰

$$\dot{\sigma}_{BI} = G(\sigma_{BI}) \omega_{BI}^B \quad (1a)$$

$$G(\sigma_{BI}) = \frac{1}{2} \left(\frac{1 - \sigma_{BI}^T \sigma_{BI}}{2} \mathbf{I}_3 + \sigma_{BI}^\times + \sigma_{BI} \sigma_{BI}^T \right)$$

$$\mathbf{J} \dot{\omega}_{BI}^B + \omega_{BI}^B \times \mathbf{J} \omega_{BI}^B = \tau_c^B + \tau_d^B \quad (1b)$$

where $\omega_{BI}^B \in \mathbb{R}^3$ denotes the angular velocity expressed in the body-fixed frame, $\mathbf{J} \in \mathbb{R}^{3 \times 3}$ is the inertia matrix, \mathbf{I}_3 denotes the identity matrix, and $(\mathbf{x})^\times$ is the 3×3 skew-symmetric cross-product matrix associated with vector $\mathbf{x} \in \mathbb{R}^3$. τ_c^B and τ_d^B represent the control torque and the disturbance, respectively.

σ_{XY} denotes the orientation of X frame relative to Y frame. ω_{YZ}^X is the angular velocity of Y frame relative to Z frame expressed in X frame. Then, the relative attitude between two frames is defined as

$$\sigma_{XY} = \frac{\sigma_{YI}(\sigma_{XI}^T \sigma_{XI} - 1) + \sigma_{XI}(1 - \sigma_{YI}^T \sigma_{YI}) - 2\sigma_{YI}^\times \sigma_{XI}}{1 + \sigma_{XI}^T \sigma_{XI} \sigma_{YI}^T \sigma_{YI} + 2\sigma_{YI}^T \sigma_{XI}}$$

and the dynamics of σ_{XY} is given by

$$\dot{\sigma}_{XY} = G(\sigma_{XY})\omega_{XY}^X \quad (2a)$$

$$J\dot{\omega}_{XY}^X + \omega_{XI}^X \times J\omega_{XI}^X - J(\omega_{XY}^X \times \omega_{YI}^X - C_Y^X \omega_{YI}^Y) = \tau_c^B \quad (2b)$$

where $\omega_{XY}^X = \omega_{XI}^X - \omega_{YI}^X$ and $\omega_{YI}^X = C_Y^X \omega_{YI}^Y$. The rotation matrix in terms of the MRPs from Y frame to X frame can be expressed as

$$C_Y^X = I_3 + \frac{8(\sigma_{XY}^\times)^2 - 4(1 - \sigma_{XY}^T \sigma_{XY})\sigma_{XY}^\times}{(1 + \sigma_{XY}^T \sigma_{XY})^2}. \quad (3)$$

The following properties will be frequently used in this paper:

$$\sigma_{XY}^T G(\sigma_{XY}) = \left(\frac{1 + \sigma_{XY}^T \sigma_{XY}}{4} \right) \sigma_{XY}^T \quad (4)$$

$$G(\sigma_{XY})^T G(\sigma) = \left(\frac{1 + \sigma^T \sigma}{4} \right)^2 I_3. \quad (5)$$

According to the description of MRPs in 28, MRPs have geometric singularities when $\phi = \pm 360^\circ$, and it is not unique because of the shadow set, i.e., $\sigma = \sigma^s$, $\sigma^s = -\sigma/\sigma^T \sigma$. Recalling the definition of σ , one knows that $\|\sigma\| \leq 1$ for all $|\phi| \leq 180^\circ$. Thus, the spacecraft attitude can be globally parameterized with the shortest principal rotation by switching the σ and σ^s at the unit sphere $\|\sigma\| = 1$. Consequently, we stipulate that the magnitude of σ is bounded by 1, i.e., $\|\sigma\| \leq 1$, which is suited to describe any reorientation.

2.2 | State and control constraints

The pointing constraint, the angular velocity constraint and the input limitation are considered in this paper. For the pointing constraint, we suppose the instantaneous angle ϑ between a body-fixed unit vector r_c^B (such as cameras) and a inertial constant unit vector r_t^I (observed target) should be maintained in a half-cone angel ϑ_m , i.e., $\theta \leq \vartheta_m$, which is equivalent to

$$C_p = \left\{ (\sigma_{BI}, \omega_{BI}^B) : r_c^B \cdot r_t^B \geq \cos(\vartheta_m), \vartheta_m \in (0, \frac{\pi}{2}) \right\} \quad (6)$$

where $r_t^B = C_I^B r_t^I$ is the expression of r_t^I in \mathcal{F}_B .

In consideration of the payload requirements, the angular velocity constraint is always exists. Then the constraint set is given by

$$C_\omega = \{(\sigma_{BI}, \omega_{BI}^B) : \|\omega_{BI}^B\| \leq \omega_{\max}, \omega_{\max} > 0\} \quad (7)$$

where $\omega_{\max} \in \mathbb{R}^+$ is the maximum angular velocity amplitude.

The angular momentum exchange devices such as reaction wheels and control moment gyros are usually used as the spacecraft attitude control actuators. These devices may be saturated when the command torque is large. For simplicity, the actuator constraint is formulated as

$$C_\tau = \{(\sigma_{BI}, \omega_{BI}^B) : \|\tau_c^B\| \leq \tau_{\max}, \tau_{\max} > 0\} \quad (8)$$

where $\tau_{\max} \in \mathbb{R}^+$ is the maximum allowable control torque.

Finally, the dynamic safety margin of the system is the intersection of the aforementioned three subsets:

$$C = C_p \cap C_\omega \cap C_\tau. \quad (9)$$

2.3 | Problem statements

This paper aims to develop a ERG control scheme that drives the system states $(\sigma_{BI}, \omega_{BI}^B)$ to the desired equilibrium $(\sigma_{DI}, \mathbf{0}_{3 \times 1})$ while satisfying the constraints (6), (7), and (8). The proposed ERG-based control structure (shown in Fig. 1) consists of two cascaded control units. The primary controller is given by an angular velocity observer-based output feedback controller, which is able to pre-stabilize the unconstrained system to an auxiliary reference σ_{VI} . The reference governor (navigation layer) unit is designed to guarantee the constraint enforcement by manipulating the kinematics of σ_{VI} . Clearly, the asymptotic convergence property of the closed-loop control system will be achieved by the goal that auxiliary reference σ_{VI} asymptotically tends to σ_{DI} . The reference attitude σ_{DI} is a constant and selected inside the admissible region, i.e., (6) is satisfied when $\sigma_{BI} = \sigma_{DI}$.

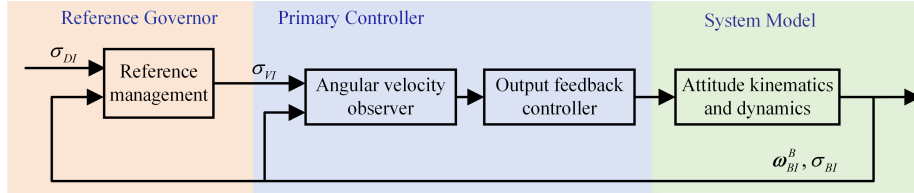


Figure 1 The architecture of the explicit reference governor based attitude control scheme.

3 | INNER LOOP OBSERVER-BASED OUTPUT FEEDBACK CONTROLLER DESIGN

This section proposes an angular velocity-free control law so as to stabilize the attitude to any constant reference $\bar{\sigma}_{VI}$ ($\dot{\sigma}_{VI} = \mathbf{0}_{3 \times 1}$) when the constraints and disturbance are neglected. The time-varying of σ_{VI} will be addressed by the reference management unit detailed in the next section.

3.1 | Observer design

The angular velocity observer is constructed based on the I&I theory^{27,31}. Let \mathcal{F}_E be the estimation frame of the \mathcal{F}_B . The attitude and angular estimation errors in terms of MRPs are given by

$$\sigma_{BE} = \frac{\sigma_{EI}(\sigma_{BI}^T \sigma_{BI} - 1) + \sigma_{BI}(1 - \sigma_{EI}^T \sigma_{EI}) - 2\sigma_{EI}^\times \sigma_{BI}}{1 + \sigma_{BI}^T \sigma_{BI} \sigma_{EI}^T \sigma_{EI} + 2\sigma_{EI}^T \sigma_{BI}} \quad (10a)$$

$$\omega_{BE}^B = \omega_{BI}^B - C_E^B \omega_{EI}^E = \omega_{BI}^B - \omega_{EI}^B. \quad (10b)$$

To ensure $\omega_{BE}^B \rightarrow 0$ and $\sigma_{BE} \rightarrow 0$, a scalar $\varpi \in \mathbb{R}^+$ that can 'cover' the ω_{EI}^B is introduced as

$$\varpi = \sqrt{\varepsilon_\omega + \|\omega_{EI}^B\|^2} \quad (11)$$

where $\varepsilon_\omega \in \mathbb{R}^+$ is a constant to be selected, which is utilized to ensure the existence of the time derivative of ϖ . Then, ω_{EI}^B is generated by

$$\omega_{EI}^B = \xi + 4J^{-1} \beta(\varpi) \sigma_{BE} \quad (12)$$

where ϖ is the estimate of ϖ , ξ and $\beta(\varpi)$ are the parameter related to ω_{EI}^B and a function of ϖ , respectively. The dynamics of ξ , ϖ , and σ_{EI} are designed as

$$\begin{aligned} \dot{\xi} = & J^{-1}(-\omega_{EI}^B \times J\omega_{EI}^B + \tau_c^B) - 4J^{-1} \dot{\beta}(\varpi) \sigma_{BE} \\ & - 4J^{-1} \beta(\varpi) \dot{\sigma}_{1BE} \end{aligned} \quad (13a)$$

$$\dot{\varpi} = \varpi^{-1} (\omega_{EI}^B)^T J^{-1} (-\omega_{EI}^B \times J\omega_{EI}^B + \tau_c^B) - K_\varpi (\varpi - \varpi) \quad (13b)$$

$$\dot{\sigma}_{EI} = G(\sigma_{EI})(\omega_{EI}^E + K_\sigma C_B^E \sigma_{BE}) \quad (13c)$$

where $K_{\underline{\omega}}$ and K_{σ} are the dynamic gains to be designed, $\dot{\sigma}_{1BE}$ represents part of the dynamics of σ_{BE} , and it can be obtained from (1a), (10a), and (13c) :

$$\dot{\sigma}_{BE} = \dot{\sigma}_{1BE} + \dot{\sigma}_{2BE} \quad (14)$$

with $\dot{\sigma}_{1BE} = -G(\sigma_{BE})K_{\sigma}\sigma_{BE}$ and $\dot{\sigma}_{2BE} = G(\sigma_{BE})\omega_{BE}^B$.

To inject the nonlinear terms in the dynamics of ω_{BE}^B a dynamic scaling technique is introduced:

$$z = \frac{\omega_{BE}^B}{r} \quad (15)$$

where r is the dynamic scaling factor and is updated by the following law

$$\dot{r} = \frac{r}{J_m}(J_M\|\underline{\omega} - \underline{\omega}\|) - \frac{k_r}{J_M}(r - 1) \quad (16)$$

where $k_r \in \mathbb{R}^+$ is the dynamic scaling gain to be determined, J_m and J_M are the minimum and the maximum eigenvalues of the inertia matrix \mathbf{J} , respectively. If $r(t) = 1$, $\dot{r} \geq 0$. Hence, it satisfies $r(t) \geq 1$ for all $t \geq 0$ when $r(0) \geq 1$. Finally, the convergence analysis of the proposed observer (12) is summarized as the following proposition.

Proposition 1. Consider the angular velocity observer in (12) with dynamics given in (13), (16), and the gains are given as

$$\beta(\underline{\omega}) = 4\beta(\underline{\omega})G^T(\sigma_{BE}) \quad (17a)$$

$$\underline{\beta}(\underline{\omega}) = J_M\|\underline{\omega}\| + \frac{J_mk_r}{J_M} + 1 + \rho_{\underline{\omega}} \quad (17b)$$

$$K_{\underline{\omega}} = 8 \left(\frac{\|\omega_{EI}^B\|\beta(\underline{\omega})r}{J_m} \right)^2 + \frac{1}{2}r^2J_M + \rho_{\underline{\omega}} \quad (17c)$$

$$K_{\sigma} = \frac{1}{2}r^2 + \rho_{\sigma} \quad (17d)$$

$$k_r = \frac{1}{2} \frac{J_M^2}{J_m} + \rho_r \quad (17e)$$

where $\rho_{\underline{\omega}}$, $\rho_{\underline{\omega}}$, ρ_{σ} , and ρ_r are positive constants that can be tuned for different convergence rates of the estimation errors. Then, the dynamic scaling factor r is bounded and the errors globally exponentially converges to the origin, i.e., $\lim_{t \rightarrow \infty} e^{\alpha t} \|\omega_{BE}^B\| = 0$, $\alpha \in \mathbb{R}^+$.

Proof: See the Appendix. ■

3.2 | Output controller design

The aforementioned angular velocity observer is used to derive an output feedback attitude controller. As shown in Fig. 1, the following theorem summarize the result on the unconstrained output controller.

Theorem 1. Consider the attitude dynamics given in (1) and the angular velocity observer given in (12)-(17). Then, the output feedback control law is given by

$$\tau_c^B = -k_p\sigma_{BV} - k_d\omega_{EI}^B \quad (18)$$

with $k_p, k_d > 0$, the equilibrium $(\bar{\sigma}_{VI}, \mathbf{0}_{3 \times 1})$ is asymptotically stable within the admissible set, i.e., $\lim_{t \rightarrow \infty} (\sigma_{BI}, \omega_{BI}^B) = (\bar{\sigma}_{VI}, \mathbf{0}_{3 \times 1})$.

Proof: By means of (10b), the control law (18) can be expressed as a full-state controller plus perturbations induced by velocity estimation error, namely,

$$\tau_c^B = -k_p\sigma_{BV} - k_d\omega_{BI}^B + k_d\omega_{BE}^B. \quad (19)$$

Consider a Lyapunov function candidate as follows:

$$V_c = 2k_p \ln(1 + \sigma_{BV}^2) + \frac{1}{2}(\omega_{BI}^B)^T \mathbf{J} \omega_{BI}^B. \quad (20)$$

Taking the time derivative of (20) along (1), (4), and (19), one can obtain

$$\begin{aligned}\dot{V}_c &= 4k_p \frac{\sigma_{BV}^T \dot{\sigma}_{BV}}{1 + \sigma_{BV}^2} + (\omega_{BI}^B)^T J \dot{\omega}_{BI}^B \\ &\leq -k_d \|\omega_{BI}^B\|^2 + k_d \|\omega_{BI}^B\| \|\omega_{BE}^B\|.\end{aligned}\quad (21)$$

Clearly, \dot{V}_c includes sign indefinite term caused by angular velocity estimation error. To eliminate this effect, let the positive definite Lyapunov function be of the following form:

$$V = V_c + \delta_z V_z \quad (22)$$

where δ_z is a positive constant to be determined. Differentiating V and applying (21) and (A4) yields

$$\begin{aligned}\dot{V} &= -k_d \|\omega_{BI}^B\|^2 + k_d \|\omega_{BI}^B\| \|\omega_{BE}^B\| - \delta_z (1 + \rho_w) \|z\|^2 \\ &\leq -[\|\omega_{BI}^B\| \|\omega_{BE}^B\|] \begin{bmatrix} k_d & -\frac{1}{2}k_d \\ -\frac{1}{2}k_d \delta_z r^{-2} (1 + \rho_w) \end{bmatrix} \begin{bmatrix} \|\omega_{BI}^B\| \\ \|\omega_{BE}^B\| \end{bmatrix}.\end{aligned}\quad (23)$$

Due to $1 \leq r < \infty$, there exists a large enough δ_z that \dot{V} is negative semi-definite for $\bar{\sigma}_{VI}$. By using the LaSalle invariance principle, one can conclude that the equilibrium point $(\bar{\sigma}_{VI}, \mathbf{0}_{3 \times 1})$ of the system is asymptotically stable. This completes the proof. \blacksquare

Obviously, σ_{VI} is time varying, Theorem 1 only provide a claim about the tracking error stability of $\bar{\sigma}_{VI}$ rather than σ_{VI} . In fact, since the final state σ_{DI} is a constant attitude, the inner loop controller only needs to ensure that the attitude can converge to the final state. In addition, the angular velocity cannot be obtained precisely, hence the angular velocity constraint is hard to be guaranteed strictly. Fortunately, the value of the dynamic scaling factor r implies the estimation error. By designing a parameters related to r , the angular velocity constraints can be satisfied. These properties will be utilized in the next section.

Remark 1. Throughout the aforementioned analysis, it can be easily checked that the design of the output feedback controller is independent of the angular velocity observer (see (18) and (19)), which greatly reduces the difficulty of the controller design. Moreover, (13) and (17) indicate that the scale of the observer gains is contradictory to the robustness. However, there are always parameter uncertainties in practical missions, so it is necessary to balance the two properties, which will be verified in detail in the simulation.

4 | REFERENCE MANAGEMENT

The reference management layer of ERG (shown in Fig. 1) designs an auxiliary control law that manipulates the reference state to the primary stabilized system^{32,18}. The objective of this part is to handle the constraints given in (6) – (8) by designing the safety margin and the navigation field, which is achieved by the invariant set in the Lyapunov function centered on the reference state σ_{VI} . The auxiliary reference is formulated as the following form:

$$\dot{\sigma}_{VI} = \Delta(\sigma_{BV}, \omega_{EI}^B) \chi(\sigma_{VI}, \sigma_{VD}) \quad (24)$$

where $\Delta(\sigma_{BV}, \omega_{EI}^B) : \mathbb{R}^3 \times \mathbb{R}^3 \rightarrow \mathbb{R}$ is the dynamic safety margin that indicates how safe it is within the allowable set. $\chi(\sigma_{VI}, \sigma_{VD}) : \mathbb{R}^3 \times \mathbb{R}^3 \rightarrow \mathbb{R}^3$ denotes the navigation field of the current state σ_{VI} , and the σ_{VD} is utilized to drive the σ_{VI} towards to σ_{DI} .

4.1 | Safety margin

Intuitively, the safety margin can be treated as the distance between the constraint boundary and the navigation field. Since \dot{V} is negative semi-definite (see (23)), the forward invariant set $\{(\sigma_{BI}, \omega_{BI}^B) : V \leq \Gamma\}$ can be used to design the safety margin, where the upper bound $\Gamma(\sigma_{VI}^V, \omega_{VI}^V)$ is determined by the constraints (6) – (8). In 19 and 21, authors design the dynamic safety margin in the form $\Delta(\sigma_{BV}, \omega_{EI}^B) = k_e(\Gamma - V)$, where the constant k_e is used to adjust the dynamic performance. Unfortunately, since the exact estimation error ω_{BE}^B is unavailable, the angular velocity can not be obtained either. In order to prevent Δ being negative

caused by ω_{BE}^B , Δ can be designed as

$$\Delta(\sigma_{BV}, \omega_{EI}^B) = \begin{cases} k_e(\Gamma - V), & \Gamma > V \\ 0, & \Gamma \leq V. \end{cases} \quad (25)$$

4.1.1 | Pointing constraint

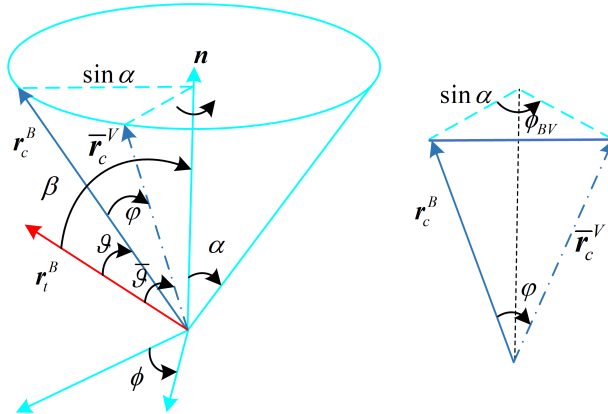


Figure 2 Constrained attitude region.

The geometric relationship about the pointing constraint is displayed in Fig. 2, where $\vartheta_e \in (0, \frac{\pi}{2})$ is the safety margin of σ_{BV}^B and satisfies $\vartheta_e = \vartheta_m - \vartheta$. When the body frame is coincided with the reference frame \mathcal{F}_V , the pointing angle $\bar{\vartheta}$ is denote by

$$\bar{\vartheta} = \arccos(\bar{\mathbf{r}}_c^V \cdot \mathbf{r}_t^V). \quad (26)$$

Note that $\bar{\mathbf{r}}_c^V = \mathbf{r}_c^B$ is a virtual constant unit vector expressed in \mathcal{F}_V rather than $\bar{\mathbf{r}}_c^V = \mathbf{C}_B^V \mathbf{r}_c^B$. Under these conditions, the safety margin of σ_{VI}^V satisfies $\bar{\vartheta}_e = \vartheta_m - \bar{\vartheta}$ and $\bar{\vartheta}_e \in (0, \frac{\pi}{2}]$. Let $\alpha \in [0, \pi]$ be the gap between \mathbf{n}_{BV} and the unit vector \mathbf{r}_c^B , then it satisfies

$$\mathbf{r}_c^B \cdot \mathbf{n}_{BV} = \cos(\alpha) \quad (27)$$

Let $\varphi \in (0, \pi)$ denote the orientation from \mathbf{r}_c^B to $\bar{\mathbf{r}}_c^V$, and they have the following relationship:

$$\sin\left(\frac{\varphi}{2}\right) = \sin\left(\frac{\phi_{BV}}{2}\right)\sin(\alpha). \quad (28)$$

Obviously, there is a positive correlation between φ and ϕ_{BV} , and they satisfies $\varphi \leq \phi_{BV}$. Since $|\vartheta_e - \bar{\vartheta}_e| \leq \varphi$, if $\varphi \leq \bar{\vartheta}_e$, then $\vartheta_e \geq 0$ can be guaranteed.

According to 6, if $\omega_{EI}^E = \mathbf{0}_{3 \times 1}$ (ω_{BI}^B is precisely known), then $\dot{V}_c = \dot{V} \leq 0$, the threshold of $V \leq \Gamma'_p$ can be designed as

$$\Gamma'_p = \begin{cases} 2k_p \ln \left\{ 1 + \left(\frac{1 - \sqrt{1 - a_p^2}}{a_p} \right)^2 \right\} & \alpha \in (0, \pi) \\ \infty & \alpha = 0 \text{ or } \pi \end{cases} \quad (29)$$

where $a_p = \sin(\frac{\bar{\vartheta}_e}{2})/\sin(\alpha)$.

When $V = \Gamma'_p$, $\dot{\sigma}_{VI} = \mathbf{0}_{3 \times 1}$. According to Theorem1, the time derivate of V and Γ'_p satisfies $\dot{V} \leq 0$, $\dot{\Gamma}'_p = 0$, which means the pointing constraint (6) will never be violated. However, ω_{BI}^B and δ_z are unavailable, which means V and V_c are unavailable, thus they can not be used to design the threshold of the pointing constraint. Hence, we replace the Lyapunov function with the following form

$$\bar{V} = 2k_p \ln(1 + \sigma_{BV}) + \frac{1}{2}(\omega_{EI}^B)^T \mathbf{J} \omega_{EI}^B. \quad (30)$$

Although $\dot{\bar{V}}$ is sign indefinite, according Theorem 1, \bar{V} is asymptotically convergent, i.e., $\lim_{t \rightarrow \infty} \bar{V}(t) = 0$. Accordingly, the threshold of the pointing constraint is designed as

$$\Gamma_p = \frac{\Gamma'_p}{r^{k_1}} \quad (31)$$

where $k_1 > 0$ is a constant parameter. Similarly to the analysis in Sec. 3.1, the larger ω_{BE}^B is, the larger r is, and the smaller Γ_p is. Although the exact relationship between ω_{BE}^B and r is unknown, by tuning k_1 , a conservative but safe threshold of the pointing constraint without angular velocity measurement can be obtained.

4.1.2 | Angular velocity constraint

The angular velocity constraint given in (7) is a convex set. As discussed in Sec. 4.1.1, when $\omega_{EI}^E = \mathbf{0}_{3 \times 1}$, the threshold of the angular velocity constraint Γ_ω can be selected as

$$\Gamma'_\omega = \frac{1}{2} J_m \omega_{\max}^2. \quad (32)$$

Similar to the pointing constraint, when $V = \Gamma'_\omega$, $\dot{\sigma}_{VI} = \mathbf{0}_{3 \times 1}$. Recalling Theorem 1, the time derivate of them satisfies $\dot{V} \leq 0$, $\dot{\Gamma}'_\omega = 0$, which means the pointing constraint (7) will never be violated. When $\omega_{EI}^E \neq \mathbf{0}_{3 \times 1}$, the Lyapunov function is replaced by (30), and the threshold can be selected as

$$\Gamma_\omega = \frac{\Gamma'_\omega}{r^{k_2}} \quad (33)$$

where $k_2 > 0$ is a constant parameter used to tuning Γ_ω .

4.1.3 | Actuator saturation

Similar with the other constraints, ω_{BI}^B is replaced by ω_{EI}^B and we omit the estimation error. Following the approach given in 21, the saturation constraint (8) can be satisfied by solving the following optimization problem

Problem

$$\min 2k_p \ln(1 + \sigma_{BV}) + \frac{1}{2} (\omega_{EI}^B)^T J \omega_{EI}^B$$

subject to

$$|\sigma_{BV}|_i \leq 1 \quad (34a)$$

$$|k_p \sigma_{BV} + k_d \omega_{EI}^B|_i \geq \tau_{\max}. \quad (34b)$$

Then the threshold Γ_τ can be obtained by taking the minimum value of the aforementioned optimization problem for $i = 1, 2, 3$. Consequently, the upper-bound of the system subject to the constraint (9) can be concluded as $\Gamma = \min\{\Gamma_p, \Gamma_\omega, \Gamma_\tau\}$, which can be proved by using the same arguments in 19.

4.2 | Navigation layer

The navigation field $\chi(\sigma_{VI}, \sigma_{VD})$ will be designed in this section to ensure that the auxiliary reference σ_{BV} converges to the desired reference σ_{BD} . Consequently, the trajectory of $\chi(\sigma_{VD})$ should lie in the allowable set \mathcal{C} strictly. Since the initial and final attitudes are all within the constraints and the pointing constraint \mathcal{C}_p is a convex set, the shortest distance on the attitude manifold obey the constraints. The navigation trajectory $\chi(\sigma_{VD})$ is designed by

$$\chi(\sigma_{VD}) = -G(\sigma_{VD})\sigma_{VD}. \quad (35)$$

Since $\omega_{BI}^B = \mathbf{0}_{3 \times 1}$ and $\tau_c^B = \mathbf{0}_{3 \times 1}$ represent the equilibrium point, the constraints (7) and (8) are always satisfied at steady-state. Then, the main results about the constrained attitude maneuver control without angular velocity measurement is presented in the following theorem.

Theorem 2. Given the spacecraft attitude dynamics (1) subject to the constraints (9) with the angular velocity observer (12) controlled by (18), and let (24) be the navigation layer subject to the dynamic safety margin (25), and the navigation field (35). Then, for any initial states satisfy the constraints and $V(0) \leq \Gamma(0)$, the following statements hold. 1) For any constant reference $\sigma_{DI} \in \mathcal{C}$, the system constraints are all satisfied. 2) The auxiliary reference σ_{VI} updated by (24) asymptotically converges to σ_{DI} .

Proof: See 6. ■

Remark 2. Combining the design process of ERG and the above analysis, it can be seen that by designing a trajectory from the current state to the final state that satisfies the constraint conditions, and then the controller drives the system state and the reference state error within a certain range, the system states can be guaranteed to reach the target state while the constraints are met. Another advantage of this strategy is that even there is no state constraint. Compared with other control algorithms (such as PID), the ERG algorithm can track the σ_{VD} independently generated by the reference management with smaller error than σ_{BD} , which can also achieve faster and more precise control performance.

5 | NUMERICAL SIMULATIONS

This section demonstrates the effectiveness of the proposed angular velocity free attitude control algorithm in the presence of multi-constraints. The operation aims to control the rigid spacecraft from a certain initial state to the per-designed target, where the attitude constraint, angular velocity constraint and the control saturation are all considered simultaneously. Besides, Monte Carlo results are conducted to further verify the robustness of the proposed control scheme. The inertia of the spacecraft is given by

$$J = \begin{bmatrix} 15.2 & -1 & 2 \\ -1 & 18.3 & -0.5 \\ 2 & -0.5 & 16.1 \end{bmatrix} \text{kg.m}^2.$$

Table 1 System Constraint Conditions.

Parameters	Values
σ_{DI}	$[0, 0, 0]^T$
ϑ_m	38°
r_t^I	$[1/\sqrt{3}, -1/\sqrt{3}, 1/\sqrt{3}]^T$
r_c^B	$[0, -1/\sqrt{2}, 1/\sqrt{2}]^T$
ω_{max}	0.035 rad/s
τ_{max}	0.1 N.m.s
k_e	1000
k_1, k_2	2

Table 2 Observer parameters.

Parameters	Values
J_m	18.3
J_M	15.2
$\rho_\sigma, \rho_\omega, \rho_{\underline{\omega}}, \rho_r, \varepsilon_\omega$	0.1
$r(0)$	1
$\xi(0)$	$[0, 0, 0]^T$
$\sigma_{EI}(0)$	$[-0.119, 0.000, 0.159]^T$
ω_{EI}^B	$[0, 0, 0]^T \text{ rad/s}$

The initial states are set as $\sigma_{BI}(0) = [-0.119, 0.000, 0.159]^T$ and $\omega(0) = [0, -0.01, 0.01]^T \text{ rad/s}$. The constraint conditions and target state are chosen in Table 1. Besides, the threshold of actuator saturation Γ_τ is obtained by solving from the *Problem* via *fmincon* function in Matlab 2021, which is 0.0468, and the observer parameters are shown in Table 2. The control elements are selected as $k_p = 1.5$ and $k_d = 2.5$. For the brevity and intuition, Euler angles $[\varphi, \vartheta, \psi]^T$ with sequence 3 – 1 – 2 are used to plot the attitude.

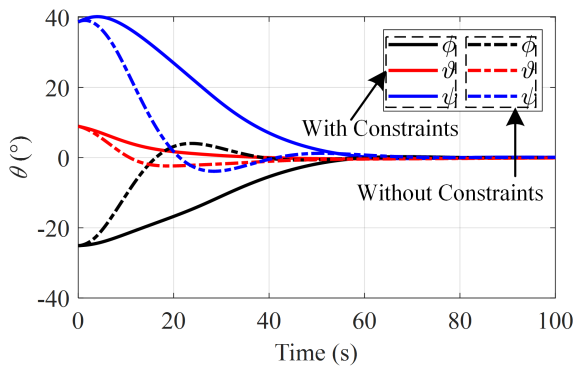


Figure 3 Attitude trajectories.

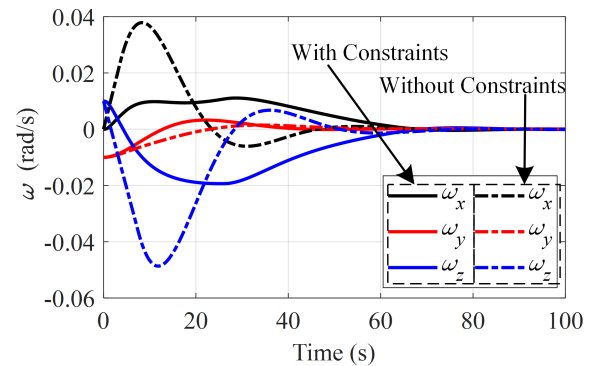


Figure 4 Angular velocities.

5.1 | Performance of the proposed control scheme

The simulation results are shown in Figs. 3 – 11, where the dash curve represents the simulation without reference management i.e., the constraints are not considered in the control scheme. The attitude trajectories and angular velocities depicted in Figs. 3 and 4 indicate that with the navigation layer, the trajectories of attitude and the velocity become smoother and the overshoot is smaller.

Fig. 5 depicts the attitude and velocity estimation errors produced by the I&I based observer designed in (12). In the logarithmic coordinate, the estimation errors $\|\omega_{BE}^B\|$ and $\|\sigma_{BE}\|$ decreases in an almost straight line, indicating that the estimation error is exponentially convergent. An interesting phenomenon is that unlike $\|\omega_{BE}^B\|$ decreases with time, $\|\sigma_{BE}\|$ is very small at the beginning, but increases first and then decreases. This is because $\|\sigma_{BE}\|$ is used to "measure" whether the estimation of $\|\omega_{BE}^B\|$ is appropriate. As we set $\|\sigma_{BE}\| = 0$ as the initial condition, and the estimation error $\|\omega_{BE}^B(0)\|$ is large, $\|\sigma_{BE}\|$ becomes larger, and as $\|\omega_{BE}^B\|$ becomes smaller, $\|\sigma_{BE}\|$ also changes accordingly. As we can also seen from Figs. 5 and 6, due to the large estimation error at the beginning, the injection gain r is also relatively large, but as the estimation error decreases, r also tends to 1 rapidly. These results mean that the inject gain r plays an important role in the observer and the performance of the observer achieved the desired effectiveness. Furthermore, the final angular velocity estimation error $\|\omega_{BE}^B(0)\|$ is about 10^{-4} , which is mainly restricted by the simulation setting 0.01s. If the step size is further reduced, $\|\omega_{BE}^B(0)\|$ can also be reduced.

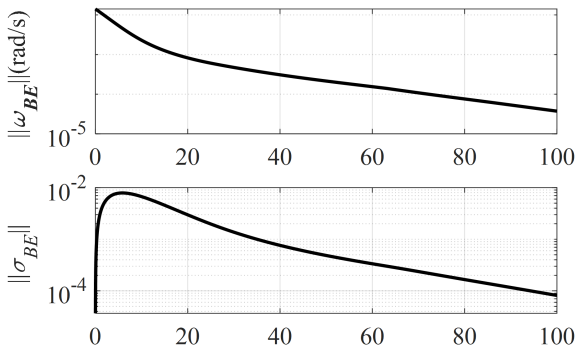


Figure 5 Attitude and Velocity estimation errors.

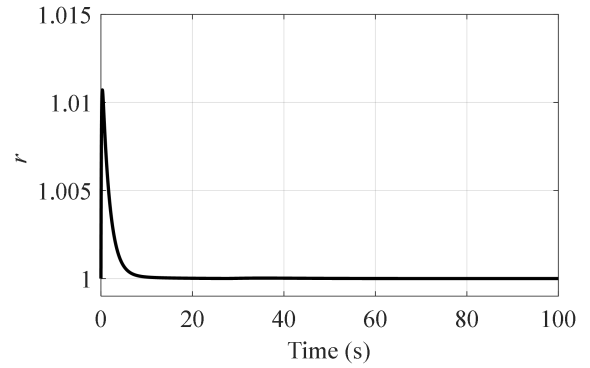


Figure 6 Injection gain r .

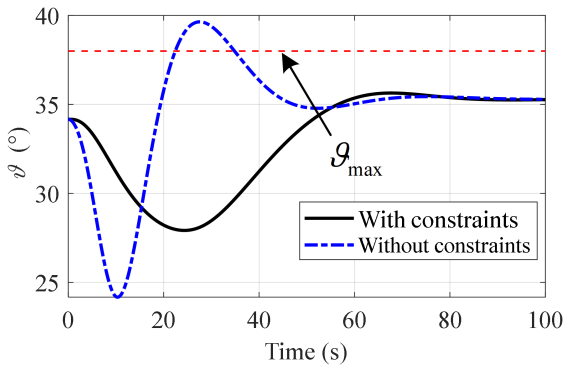


Figure 7 Pointing constraint.

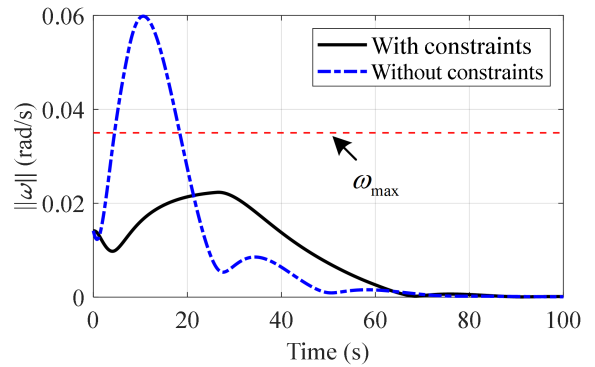


Figure 8 Angular velocity constraint.

The pointing constraint, angular velocity constraint and the control torque limitation are plotted in Figs. 7 – 9. Obviously, without reference management, the pointing angle overflow the boundary at 23 seconds and the angular velocity exceeds the limitation about 15 seconds. Also, the actuator is saturated in the first 10 seconds. When the navigation layer in applied in the

algorithm, all of the three constraints are away from the boundary. This is because the tracking error can always maintains a small error relative to the reference trajectories (see Fig. 10). Combining Figs. 10 and 11, it can be seen that the convergence speed of the reference trajectory is basically the same as the threshold error $\Gamma - V$. Generally, the simulation results are in line with the theoretical analysis, verifying the effectiveness of the algorithm.

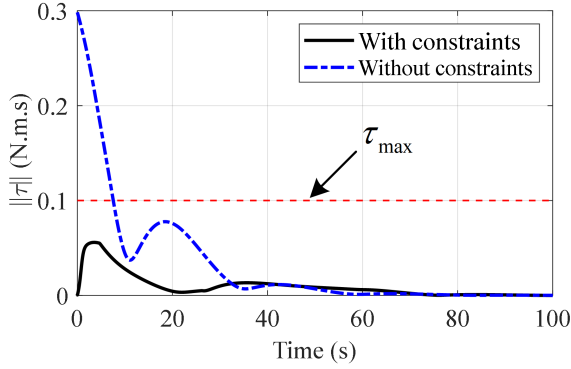


Figure 9 Control torque limitation.

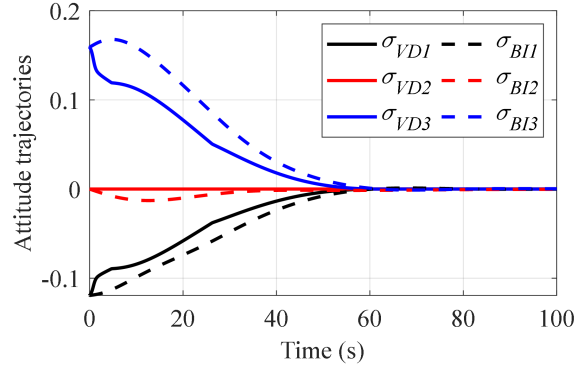


Figure 10 Reference trajectories.

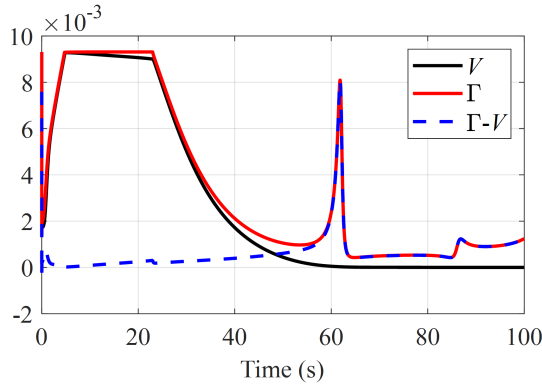


Figure 11 Threshold value.

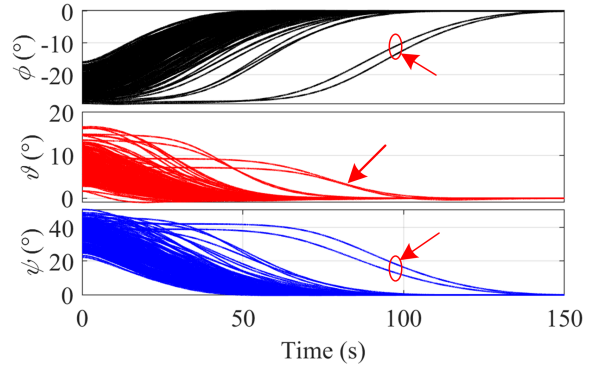


Figure 12 Attitude trajectories.

5.2 | Monte Carlo simulation under disturbances

The aforementioned section demonstrated the numerical simulation without any disturbance i.e., $\tau_d^B = \mathbf{0}_{3 \times 1}$. In this section, Monte Carlo simulations with disturbances are conducted to illustrate the robustness of the proposed ERG based attitude control scheme. To proceed with Monte Carlo simulations, the randomized initial conditions and parameters are shown in table 3. Combine with these new initial states and parameters with others simulation conditions selected in the aforementioned section, 200 Monte Carlo simulations are conducted. In order to ensure that all the cases can reach the final states, those cases that do not meet the constraints at the initial moment will be eliminated, and the simulation lasts for 150 seconds. Besides, the external disturbances are given as follows

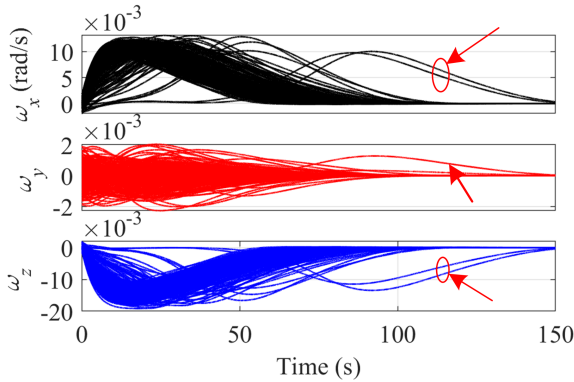
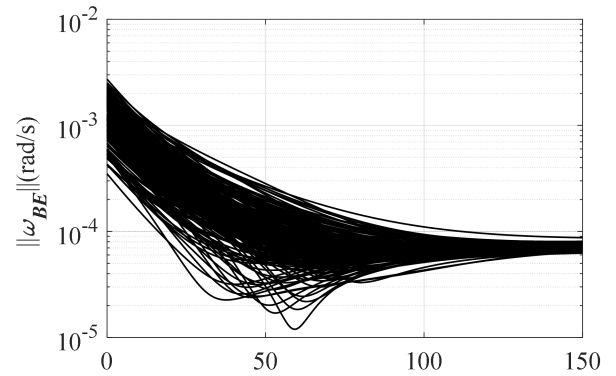
$$\tau_d^I = \begin{pmatrix} 2 \\ -1 \\ -3 \end{pmatrix} + \begin{pmatrix} 0.4\sin(\omega_A t + 1.6) \\ 2\sin(\omega_A t + 1.1) \\ 0.7\sin(\omega_A t - 2.1) \end{pmatrix} \times 10^{-5} \text{ N.m}^2$$

where $\omega_{At} = 0.01 \text{ rad/s}$.

Table 3 Randomized initial states and parameters.

Variables	Ranges
Variables	Ranges
$\mathbf{n}_1(0)$	$[-0.7, -0.5] \times [-0.1, 0.1] \times [0.7, 0.9]$
$\phi(0)$, rad	$[0.15\pi, 0.35\pi]$
$\boldsymbol{\omega}(0)$, rad/s	$\{[-2, 2] \times [-2, 2] \times [-2, 2]\} \times 10^{-3}$
\mathbf{J}_m	$[13, 17]$
\mathbf{J}_M	$[15, 21]$
$k_p = 1.5$	$[1, 1.5]$
$k_d = 2.5$	$[2.5, 3.0]$
$k_e = 1000$	$[900, 1100]$

Figs. 12 and 13 depict the attitude and angular velocity trajectories of Monte Carlo simulations. Evidently, despite the external disturbances and angular velocity estimation errors affect the control performance, the spacecraft reached the desired attitude smoothly. It can be seen from (12) and (13) that the estimation errors are affected by the precision of the input torque. Due to the unknown disturbance in the Monte Carlo simulation, the angular velocity estimation errors given in Figs. 14 and 15 are slightly larger than that in Fig. 5, but they are still very small. This shows that the observer designed in (12) can estimate angular velocity with pleased robustness. Besides, the three constraints are basically satisfied during the simulation (see Figs. 16 – 18). Meanwhile, one can also see that the angular velocity observer is independent of the controller. No matter what constraints the system needs to meet, the observer can converge without being affected by them. This interesting property helps us not be limited by the observer when we further improve the ERG-based constrained controller.

**Figure 13** Angular velocity trajectories.**Figure 14** Angular velocity estimation errors.

The fly in the ointment is that there are two cases convergent slowly (see Figs.12, 13, 16 and 17). This is because these two cases are at the edge of the pointing constraint at the initial moment. Due to external disturbances and angular velocity estimation errors, the pointing angle slightly overflows the boundary. Fortunately, the algorithm designed in this paper takes these effects into account via the improved safety margin form (25), the pointing angle can be quickly pulled back. If this situation should be strictly avoided, we only need to increase the margin of the reference state, which will be discussed in depth in our further research. In spite of this, the proposed ERG-based constrained controller still accomplished the maneuver objective with excellent accuracy, which in turn demonstrates its robustness against uncertainties.

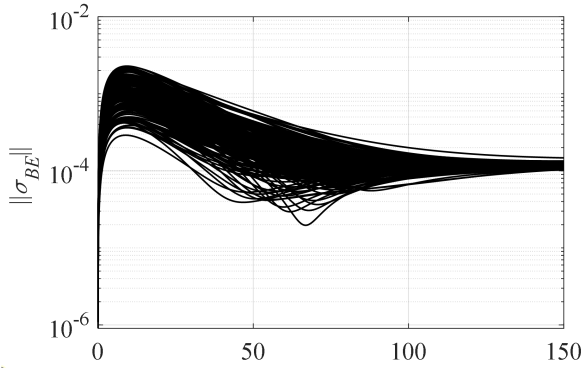


Figure 15 Attitude estimation errors.

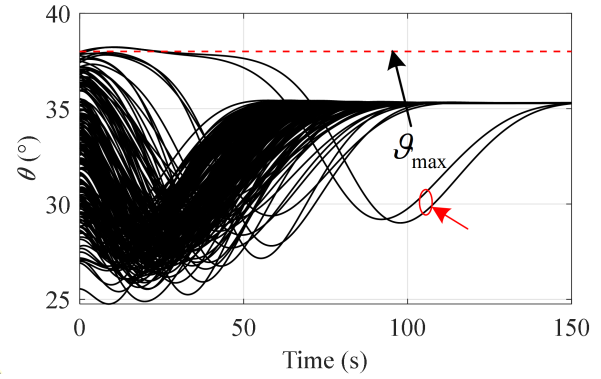


Figure 16 Distributions of pointing angles.

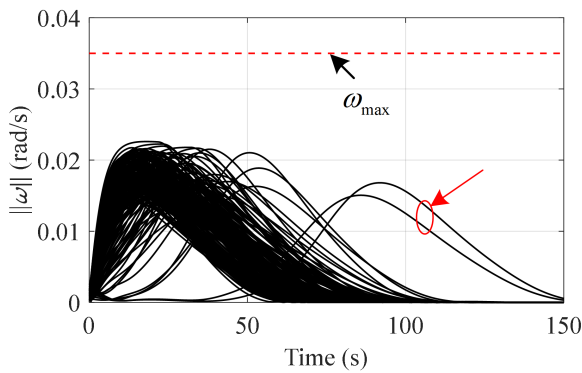


Figure 17 Distributions of angular velocity constraints.

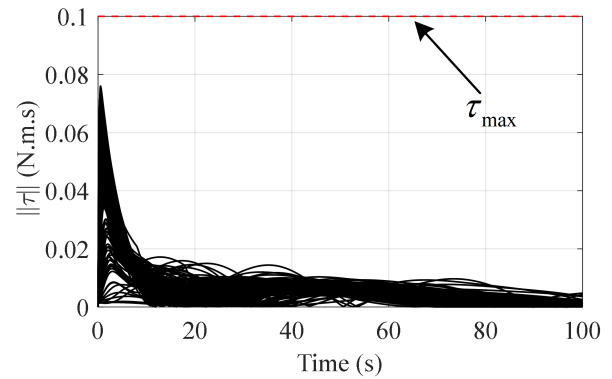


Figure 18 Distributions of control torque.

6 | CONCLUSION

This paper develop a constrained output feedback attitude reorientation problem via ERG and I&I technologies, where pointing constraint, angular velocity constraint, and the control saturation are considered. The stability of a angular velocity observer and the output feedback controller is roughly proved. The inner loop of ERG is conducted by the angular velocity observer-based output feedback controller, and the navigation layer is designed by manipulating the auxiliary reference state without violating the constraints while asymptotically converges to the desired reference. The performance of the proposed angular velocity observer and the ERG are analyzed and discussed by numerical simulations in detail.

ACKNOWLEDGMENTS

This work was partially supported by the National Natural Science Foundation of China (Grant No. 11972056), the National Key R&D Program of China (Project No. 2020YFC2200800, Task No. 2020YFC2200801), the Fundamental Research Funds for the Central Universities (Grant No. G2022WD01003), and the Natural Science Foundation of Shaanxi Province (Grant No. 2023-JC-QN-0003).

Conflict of interest

The authors declare no potential conflict of interests.

How to cite this article: Williams K., B. Hoskins, R. Lee, G. Masato, and T. Woollings (2016), A regime analysis of Atlantic winter jet variability applied to evaluate HadGEM3-GC2, *Q.J.R. Meteorol. Soc.*, 2017;00:1–6.

APPENDIX

A PROOF OF PROPOSITION1

Proof: The proposition1 can be proven by Lyapunov method by two steps. This first step is prestabilizing the inject estimation error \mathbf{z} . The second step is ensuring the dynamic scaling r is bounded.

The Lyapunov function candidate about the \mathbf{z} is chosen as

$$V_z = \frac{1}{2} \mathbf{z}^T \mathbf{J} \mathbf{z}. \quad (\text{A1})$$

The dynamics of ω_{EI}^B can be obtained from (12), (13a), (14) that

$$\dot{\omega}_{EI}^B = \mathbf{J}^{-1}(-\omega_{EI}^B \times \mathbf{J} \omega_{EI}^B + \tau_c^B) + 4\mathbf{J}^{-1} \beta(\underline{\omega}) \dot{\sigma}_{2BE}. \quad (\text{A2})$$

One can derive the dynamics of ω_{BE}^B from (1b), (10b), and (A2) that

$$\dot{\omega}_{BE}^B = \mathbf{J}^{-1}(\omega_{EI}^B \times \mathbf{J} \omega_{EI}^B - \omega_{BI}^B \times \mathbf{J} \omega_{BI}^B) - 4\mathbf{J}^{-1} \beta(\underline{\omega}) \dot{\sigma}_{2BE}. \quad (\text{A3})$$

Then, by invoking (5), (16) (17a), and (17b) and using the inequalities $\|\omega_{EI}^B\| \leq \varpi$, $\|\mathbf{a}\| \leq \|\mathbf{a}-\mathbf{b}\| + \|\mathbf{b}\|$, and $2\mathbf{a}\mathbf{b} \leq \|\mathbf{a}\|^2 + \|\mathbf{b}\|^2$, the time derivative of V_z along (15) and (A3) can be obtained as

$$\begin{aligned} \dot{V}_z &= \mathbf{z}^T \mathbf{J} r^{-1} \mathbf{J}^{-1} (\omega_{EI}^B \times \mathbf{J} \omega_{EI}^B - \omega_{BI}^B \times \mathbf{J} \omega_{BI}^B) \\ &\quad - \mathbf{z}^T \mathbf{J} r^{-1} \{4\mathbf{J}^{-1} \beta(\underline{\omega}) \dot{\sigma}_{2BE} + \dot{r}^{-1} \omega_{BE}^B\} \\ &\leq \mathbf{z}^T \left(\omega_{EI}^B \times \mathbf{J} \mathbf{z} - \beta(\underline{\omega}) \mathbf{z} \right) - r^{-1} \mathbf{z}^T \mathbf{J} \dot{\mathbf{z}} \\ &\leq J_M \|\underline{\omega}\| \|\mathbf{z}\|^2 - \beta(\underline{\omega}) \|\mathbf{z}\|^2 + \frac{J_m k_r}{J_M} \|\mathbf{z}\|^2 \\ &= -(1 + \rho_\omega) \|\mathbf{z}\|^2 \end{aligned} \quad (\text{A4})$$

which implies \mathbf{z} converges to zeros exponentially.

To show the boundedness of r , consider

$$V_o = V_z + V_\varpi + V_\sigma + V_r \quad (\text{A5})$$

where

$$\begin{aligned} V_\varpi &= \frac{1}{2} (\varpi - \underline{\omega})^2 \\ V_\sigma &= 2 \ln(1 + \sigma_{BE}^2) \\ V_r &= \frac{J_m}{2} (r - 1)^2. \end{aligned}$$

Using (11) and (A2), the dynamics of ϖ is derived as

$$\begin{aligned} \dot{\varpi} &= \varpi^{-1} (\omega_{EI}^B)^T \dot{\omega}_{EI}^B \\ &= \varpi^{-1} (\omega_{EI}^B)^T \mathbf{J}^{-1} \{-\omega_{EI}^B \times \mathbf{J} \omega_{EI}^B + \tau_c^B + 4\beta(\underline{\omega}) \dot{\sigma}_{2BE}\}. \end{aligned} \quad (\text{A6})$$

From (13b) and (A6), it follows that

$$\dot{\varpi} - \underline{\dot{\varpi}} = \varpi^{-1} (\omega_{EI}^B)^T 4\mathbf{J}^{-1} \beta(\underline{\omega}) \dot{\sigma}_{2BE} - K_\varpi (\varpi - \underline{\omega}) \quad (\text{A7})$$

Take the time derivative of V_ϖ along (A7), one can obtain

$$\begin{aligned} \dot{V}_\varpi &= (\varpi - \underline{\omega}) \left\{ \varpi^{-1} (\omega_{EI}^B)^T 4\mathbf{J}^{-1} \beta(\underline{\omega}) \dot{\sigma}_{2BE} - K_\varpi (\varpi - \underline{\omega}) \right\} \\ &\leq \frac{1}{2} \mathbf{z}^2 - (\varpi - \underline{\omega})^2 \left\{ K_\varpi - 8 \left(\frac{\|\omega_{EI}^B\| \beta(\underline{\omega}) r}{J_m \varpi} \right)^2 \right\} \end{aligned} \quad (\text{A8})$$

Applying (14) and (4), one has

$$\begin{aligned}\dot{V}_\sigma &= \frac{4\sigma_{BE}^T}{1 + \sigma_{BE}^2} G(\sigma_{BE})(\omega_{BE}^B - K_\sigma \sigma_{BE}) \\ &\leq \frac{1}{2} \dot{z}^2 - \left(K_\sigma - \frac{1}{2} r^2\right) \|\sigma_{BE}\|^2\end{aligned}\quad (A9)$$

Additionally, following the calculations in (16), one can obtain

$$\begin{aligned}\dot{V}_r &= J_m(r-1) \left\{ \frac{r}{J_m} (J_M \|\varpi - \underline{\varpi}\|) - \frac{k_r}{J_M} (r-1) \right\} \\ &\leq \frac{1}{2} \dot{z}^2 J_M \|\varpi - \underline{\varpi}\|^2 - \left(\frac{J_m k_r}{J_M} - \frac{1}{2} J_M \right) (r-1)^2\end{aligned}\quad (A10)$$

Finally, differentiating V_o along (A4), (A8), (A9), and (A10), yields

$$\dot{V}_o \leq -\rho_\varpi \|z\|^2 - \rho_{\underline{\varpi}} (\varpi - \underline{\varpi})^2 - \rho_\sigma \|\sigma_{BE}\|^2 - \rho_r (r-1)^2 \quad (A11)$$

which implies that the system is exponentially stable and r is bounded. This completes the proof.

References

1. Wei C, Chen Q, Liu J, Yin Z, Luo J. An overview of prescribed performance control and its application to spacecraft attitude system. *Proceedings of the Institution of Mechanical Engineers, Part I: Journal of Systems and Control Engineering* 2021; 235(4): 435-447.
2. Liu P, Xue W, Chen S, Huang Y, Sun Z. Integrated solution to ACMM problem of spacecraft with inertia uncertainty. *International Journal of Robust and Nonlinear Control* 2018; 28(17): 5575-5589.
3. Hu Q, Huo X, Xiao B. Reaction wheel fault tolerant control for spacecraft attitude stabilization with finite-time convergence. *International Journal of Robust and Nonlinear Control* 2013; 23(15): 1737-1752.
4. Hablani HB. Attitude Commands Avoiding Bright Objects and Maintaining Communication with Ground Station. *Journal of Guidance, Control, and Dynamics* 1999; 22(6): 759-767.
5. Cui H, Cheng X. Anti-unwinding attitude maneuver control of spacecraft considering bounded disturbance and input saturation. *SCIENCE CHINA Technological Sciences* 2012; 55(9): 2518-2529.
6. Dang Q, Liu K, Wei J. Explicit reference governor based spacecraft attitude reorientation control with constraints and disturbances. *Acta Astronautica* 2022; 190: 455-464.
7. Hu J, Zhang H. Bounded Output Feedback of Rigid-Body Attitude via Angular Velocity Observers. *Journal of Guidance, Control, and Dynamics* 2013; 36(4): 1240-1248.
8. Kjellberg HC, Lightsey EG. Discretized Constrained Attitude Pathfinding and Control for Satellites. *Journal of Guidance, Control, and Dynamics* 2013; 36(5): 1301-1309.
9. Wie B, Bailey D, Heiberg C. Rapid Multitarget Acquisition and Pointing Control of Agile Spacecraft. *Journal of Guidance Control Dynamics* 2002; 25(1): 96-104.
10. Lee U, Mesbahi M. Feedback control for spacecraft reorientation under attitude constraints via convex potentials. *IEEE Transactions on Aerospace and Electronic Systems* 2014; 50(4): 2578-2592.
11. Cheng Y, Ye D, Sun Z, Zhang S. Spacecraft reorientation control in presence of attitude constraint considering input saturation and stochastic disturbance. *Acta Astronautica* 2018; 144: 61-68.
12. Mengali G, Quarta AA. Spacecraft control with constrained fast reorientation and accurate pointing. *The Aeronautical Journal* 2004; 108(1080): 85-91.

13. Kulumani S, Lee T. Constrained geometric attitude control on SO (3). *International Journal of Control, Automation and Systems* 2017; 15(6): 2796–2809.
14. Hu Q, Chi B, Akella MR. Anti-Unwinding Attitude Control of Spacecraft with Forbidden Pointing Constraints. *Journal of Guidance, Control, and Dynamics* 2019; 42(4): 822-835.
15. Shen Q, Yue C, Goh CH, Wu B, Wang D. Rigid-body attitude stabilization with attitude and angular rate constraints. *Automatica* 2018; 90: 157 - 163.
16. Kalabić UV, Gupta R, Cairano SD, Bloch AM, Kolmanovsky IV. MPC on Manifolds with An Application to the Control of Spacecraft Attitude on SO(3). *Automatica* 2017; 76: 293 - 300.
17. Lee DY, Gupta R, Kalabić UV, et al. Geometric Mechanics Based Nonlinear Model Predictive Spacecraft Attitude Control with Reaction Wheels. *Journal of Guidance, Control, and Dynamics* 2017; 40(2): 309-319.
18. Nicotra MM, Garone E. The Explicit Reference Governor: A General Framework for the Closed-Form Control of Constrained Nonlinear Systems. *IEEE Control Systems Magazine* 2018; 38(4): 89-107.
19. Garone E, Nicotra MM. Explicit Reference Governor for Constrained Nonlinear Systems. *IEEE Transactions on Automatic Control* 2016; 61(5): 1379-1384.
20. Hosseinzadeh M, Garone E. An Explicit Reference Governor for the Intersection of Concave Constraints. *IEEE Transactions on Automatic Control* 2020; 65(1): 1-11.
21. Nicotra MM, Liao-McPherson D, Burlion L, Kolmanovsky IV. Spacecraft Attitude Control With Nonconvex Constraints: An Explicit Reference Governor Approach. *IEEE Transactions on Automatic Control* 2020; 65(8): 3677-3684.
22. Nicotra M, Garone E. *Constrained Control of Nonlinear Systems: The Explicit Reference Governor and its Application to Unmanned Aerial Vehicles*. PhD thesis. Universite Libre de Bruxelles, 2016.
23. Liu C, Shi K, Yue X, Sun Z. Inertia-free saturated output feedback attitude stabilization for uncertain spacecraft. *International Journal of Robust and Nonlinear Control* 2020; 30(13): 5101-5121.
24. Schlanbusch R, Ingar Grotli EI. Hybrid Certainty Equivalence Control of Rigid Bodies with Quaternion Measurements. *IEEE Transactions on Automatic Control* 2015; 60(9): 2512-2517.
25. Yang S, Akella MR, Mazenc F. Immersion and Invariance Observers for Gyro-Free Attitude Control Systems. *Journal of Guidance Control Dynamics* 2016; 39(11): 2567-2574.
26. Shen Q, Yue C, Goh CH. Velocity-Free Attitude Reorientation of a Flexible Spacecraft with Attitude Constraints. *Journal of Guidance, Control, and Dynamics* 2017; 40(5): 1293-1299.
27. Romero JG, Ortega R, Sarras I. A Globally Exponentially Stable Tracking Controller for Mechanical Systems Using Position Feedback. *IEEE Transactions on Automatic Control* 2015; 60(3): 818-823.
28. Junkins JL, Schaub H. *Analytical mechanics of space systems*. American Institute of Aeronautics and Astronautics . 2009.
29. Gui H, Vukovich G. Adaptive integral sliding mode control for spacecraft attitude tracking with actuator uncertainty. *Journal of the Franklin Institute* 2015; 352(12): 5832 - 5852.
30. Diaz Ramos M, Schaub H. Kinematic Steering Law for Conically Constrained Torque-Limited Spacecraft Attitude Control. *Journal of Guidance, Control, and Dynamics* 2018; 41(9): 1990-2001.
31. Dang Q, Gui H, Wen H. Dual-Quaternion-Based Spacecraft Pose Tracking with a Global Exponential Velocity Observer. *Journal of Guidance, Control, and Dynamics* 2019; 42(9): 2106-2115.
32. Bemporad A. Reference governor for constrained nonlinear systems. *IEEE Transactions on Automatic Control* 1998; 43(3): 415-419.